CHIN. PHYS. LETT. Vol. 38, No. 8 (2021) 087701

Narrow Waveguide Based on Ferroelectric Domain Wall

Gongzheng Chen(陈恭正)[1,2], Jin Lan(兰金)[1,3*], Tai Min(闵泰)[4], and Jiang Xiao(萧江)[1,2,5*]

[1]*Department of Physics and State Key Laboratory of Surface Physics, Fudan University, Shanghai 200433, China*
[2]*Institute for Nanoelectronics Devices and Quantum Computing, Fudan University, Shanghai 200433, China*
[3]*Center for Joint Quantum Studies and Department of Physics, School of Science, Tianjin University, Tianjin 300072, China*
[4]*Center for Spintronics and Quantum System, State Key Laboratory for Mechanical Behavior of Materials, School of Materials Science and Engineering, Xi'an Jiaotong University, Xi'an 710049, China*
[5]*Shanghai Research Center for Quantum Sciences, Shanghai 201315, China*

(Received 19 April 2021; accepted 4 June 2021; published online 2 August 2021)

Ferroelectric materials are spontaneous symmetry breaking systems that are characterized by ordered electric polarizations. Similar to its ferromagnetic counterpart, a ferroelectric domain wall can be regarded as a soft interface separating two different ferroelectric domains. Here we show that two bound state excitations of electric polarization (polar wave), or the vibration and breathing modes, can be hosted and propagate within the ferroelectric domain wall. In particular, the vibration polar wave has zero frequency gap, thus is constricted deeply inside ferroelectric domain wall, and can even propagate in the presence of local pinnings. The ferroelectric domain wall waveguide as demonstrated here offers a new paradigm in developing ferroelectric information processing units.

DOI: 10.1088/0256-307X/38/8/087701

A waveguide, or a structure to guide wave along designated direction without loss, is one of the basic devices for wave manipulation. The construction of waveguide lies in the heart of wave-based technologies, including optics, acoustics, magnonics, etc.[1−5] Conventionally, waveguides are built upon a heterostructure consisting of different materials, which possess distinct dispersions. As the most prominent applications, optical fibers that are based on glasses of different refraction indices have now become the standard infrastructure of the modern information society.[2]

The downscaling of waveguides is crucial for the miniaturization of information processing devices, but is much impeded by the fabrication limit of the sharp interfaces. An alternative approach is to make use of the existing interfaces that widely exist in ordered systems, including ferroelectric, ferromagnetic and multiferroic materials.[6] In ferromagnets, the magnetic domain wall, which is an interface between different magnetized domains, can be as narrow as tens of nanometers, due to the strong Heisenberg exchange coupling.[7,8] Recently, the magnetic domain wall has been shown to act naturally as a waveguide for spin wave, in both theoretical proposals and experimental observations.[5,9,10] In addition, since the magnetic domain wall is easy to create, move or eliminate, it endows the waveguide with additional flexibility.[11−14]

The ferroelectric domain wall is an interface between regions of different electric polarizations, and its characteristic size is typically smaller than its magnetic counterpart.[6,15,16] Moreover, the collective wave-like excitation of the electric polarization, similar to spin wave, has recently attracted remarkable interest, both theoretical and experimental.[17−20] Despite their close similarities with magnetic systems, systematic investigations of wave propagation along the ferroelectric domain wall are only performed in limited cases.[18]

In this Letter, we investigate the dynamics of electric polarizations upon the background of a ferroelectric domain wall. We show that two bound state modes, which correspond to the vibration and breathing of the domain wall, develop inside the domain wall. Moreover, the propagation of these polar waves along the domain wall is robust against local pinnings, as verified by numerical simulations. The functionality of the guiding polar wave enlists the ferroelectric domain wall as a new member of domain wall waveguide family.

Model. Consider a one-dimensional ferroelectric wire along the x direction, with its ferroelectric order pointing along z direction and its strength is denoted by the electric polarization p. The dynamics of the electric polarization $p(x,t)$ is governed by the Landau–Khalatinikov–Tani (LKT) equation[17,19,21−27]

$$m\frac{\mathrm{d}^2p}{\mathrm{d}t^2} = -\gamma\frac{\mathrm{d}p}{\mathrm{d}t} + \kappa\nabla^2 p - \frac{\partial V}{\partial p} + E, \qquad (1)$$

where m is the effective mass, κ is Ginzburg-type cou-

Supported by the National Natural Science Foundation of China (Grant No. 11904260), the Natural Science Foundation of Tianjin (Grant No. 20JCQNJC02020), the Science and Technology Commission of Shanghai Municipality (Grant No. 20JC1415900), and Shanghai Municipal Science and Technology Major Project (Grant No. 2019SHZDZX01).
*Corresponding authors. Email: lanjin@tju.edu.cn; xiaojiang@fudan.edu.cn
© 2021 Chinese Physical Society and IOP Publishing Ltd

pling constant between neighboring polarization, $V(p)$ is the Landau phenomenological potential as a function of polarization p, E applied along z is the external electrical field, and γ is the damping constant. Instead of the relaxational kinetics formulated in the Ginzburg-Landau equation, the inertial dynamics formulated in Eq. (1) is employed here to describe the GHz-THz dynamics of the electric polarization.

For a uniaxial ferroelectric material, as considered in this work, the Landau phenomenological potential takes the minimal p^4 form, i.e., $V(p) = -\alpha p^2/2 + \beta p^4/4$. When the two phenomenological parameters $\alpha, \beta > 0$ are positive, this potential leads to spontaneous ferroelectricity with two possible saturation electric polarizations $p = \pm P = \pm\sqrt{\alpha/\beta}$ in the absence of external electrical field ($E = 0$). Besides the Landau and Ginzburg energies, the elastic and dipolar energies also generally exist in the free energy of ferroelectric systems.[19] For the uncharged domain wall and its small oscillations under investigation here, the main contributions of both elastic and dipolar interactions are to renormalize the Landau parameters,[28–30] and thus are not explicitly included in this work.

A ferroelectric domain wall forms when two domains with different saturation polarizations meet.[31] In the present case, the ferroelectric domain wall formed with two domains with $p = \pm P$ typically has an Ising-type profile[22,23,32] as depicted in Fig 1(a) with its polarization strength varying as

$$p_0(x) = P \tanh \frac{x - X}{W}, \tag{2}$$

where X denotes the central position of domain wall, and the W is the characteristic width. In the absence of the external electric field E, the characteristic width is $W_0 = \sqrt{2\kappa/\alpha}$.[22,23]

Polar Waves within the Ferroelectric Domain Wall. The magnitude of the electric polarization may also fluctuate about its equilibrium point, and leads to wave-like excitations,[17,19,20] which is called the *polar wave* here. Separating the static and dynamical component of the polarization order parameter by $p(x,t) = p_0(x) + p'(x,t)$, where $p_0(x)$ is the static ferroelectric domain wall profile, and $p'(x,t)$ is the superimposed polar wave. In the linear regime $|p'| \ll P$, Eq. (1) reduces to a Klein–Gordon-like equation for $p'(x,t)$,

$$-m\frac{\partial^2}{\partial t^2}p' = \Big[-\kappa\frac{\partial^2}{\partial x^2} + 2\alpha + U(x)\Big]p'. \tag{3}$$

Here $U(x) = -3\alpha\text{sech}^2(x/W)$ is the effective potential accounting for the inhomogeneous domain wall profile $p_0(x)$.

When the ferroelectric wire has only one homogeneous domain (no domain wall): $U = 0$, Eq. (3) gives the bulk dispersion for polar wave: $\omega_k^2 = \omega_0^2 + (\kappa/m)k^2$, with k the wave-vector and $\omega_0 = \sqrt{2\alpha/m}$ the polar wave gap. When there is a domain wall, the domain wall induced potential well $U(x)$ is a special index-2 Pöschl–Teller potential well,[33] which hosts two bound-state polar wave modes of different symmetries within domain wall. The frequencies and profiles of the symmetric and anti-symmetric bound states are

$$\text{sym.}: \omega_\text{s} = 0, \quad p'_\text{s} \propto \text{sech}^2\frac{x}{W_0}, \tag{4a}$$

$$\text{anti-sym.}: \omega_\text{a} = \frac{\sqrt{3}}{2}\omega_0, \quad p'_\text{a} \propto \text{sech}\frac{x}{W_0}\tanh\frac{x}{W_0}. \tag{4b}$$

The spatial profiles of these two modes are shown by the solid curves in Fig. 1(b).

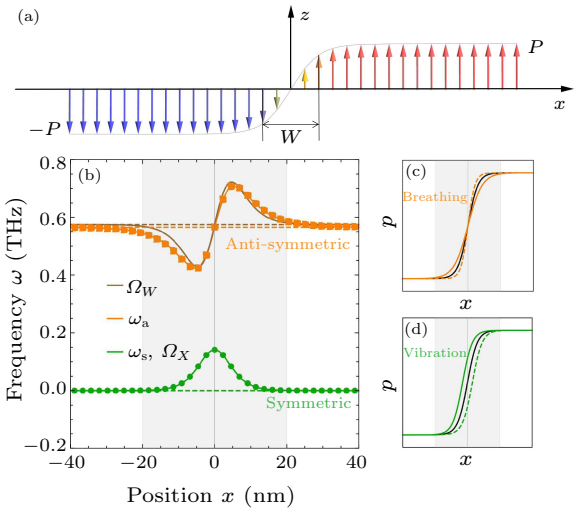

Fig. 1. Ferroelectric domain wall and its bound state modes. (a) Typical profile of the ferroelectric domain wall. The direction and length of the arrows denote the local electric polarization direction and strength, and the red/blue colors represent the up/down domains. (b) The bound state polar waves and soft modes in the ferroelectric domain wall. The green/orange lines plot the symmetric and anti-symmetric bound state polar waves, the corresponding frequency level is indicated by dashed lines, while results of numerical simulations are represented by dots. [(c), (d)] The total domain wall profile for the symmetric vibration mode and the anti-symmetric breathing mode.

Soft Modes of Ferroelectric Domain Wall. The bound state modes given in Eq. (4) can also be regarded as the soft modes of the domain wall distortion, as shown in Figs. 1(c) and 1(d). The symmetric mode, as a zero-energy Goldstone mode that costs no energy, corresponds to the vibration of the domain wall center; while the anti-symmetric mode, with finite frequency, corresponds to the breathing mode of the domain wall with oscillating width. The profiles of these two soft modes emerging from the perturbation of position X and the width W are described by an effective charge distribution as

$$q_x(x) \equiv \frac{\partial p_0}{\partial X} = -\frac{P}{W_0}\text{sech}^2\frac{x}{W_0}, \tag{5a}$$

$$q_w(x) \equiv \frac{\partial p_0}{\partial W} = -\frac{P}{W_0^2}x\,\text{sech}^2\frac{x}{W_0}. \tag{5b}$$

The soft mode q_X has symmetric charge distribution and corresponds to the vibration mode in oscillation of position X, and the soft mode q_W has anti-symmetric charge distribution and corresponds to the breathing mode in oscillation of width W.

In the basis of soft modes q_X and q_W, the domain wall dynamics in LKT Eq. (1) can be reduced to the dynamics of central position $X(t)$ and width $W(t)$ governed by

$$m_X\frac{\partial^2 X}{\partial t^2}+\gamma_X\frac{\partial X}{\partial t}=0, \tag{6a}$$

$$m_W\frac{\partial^2 W}{\partial t^2}+\gamma_W\frac{\partial W}{\partial t}=\frac{\alpha^2}{3\beta}\Big(\frac{W_0^2}{W^2}-1\Big)\equiv R(W), \tag{6b}$$

where $m_X=4mP^2/3W_0$ and $\gamma_X=4\gamma P^2/3W_0$ are effective mass and viscosity of the vibration mode, $m_W=(\pi^2-6)mP^2/9W_0$ and $\gamma_W=(\pi^2-6)\gamma P^2/9W_0$ are the effective mass and viscosity of the breathing mode, and $R(W)$ is the restoring force on width W. In Eq. (6), the dynamics for domain wall position $X(t)$ and width $W(t)$ can be fully decoupled, indicating that they are two independent degrees of freedom of a ferroelectric domain wall. According to Eq. (6a), the position X of the domain wall is arbitrary, thus the vibration mode has zero frequency $\Omega_X=0$; while in Eq. (6b), the width W always tends to restore to its equilibrium value W_0, thus the breathing mode has finite frequency $\Omega_W=\sqrt{6\alpha/m(\pi^2-6)}$.

The vibration and breathing modes of the domain wall coincide with two bound state modes discussed earlier with $\omega_{\rm s}=\Omega_X$ and $\omega_{\rm a}\simeq\Omega_W$. The profile of the vibration mode q_X is the same as the symmetric polar wave $p'_{\rm s}$; while the profile for the breathing mode q_W is also approximately the same as $p'_{\rm a}$ of the anti-symmetric polar wave, as shown in Fig. 1(b). The agreement between domain wall soft modes and the bound state polar waves is expected because they are the same physical excitations of the ferroelectric domain wall viewed from different perspectives. The slight deviation in frequency/profile between the domain wall breathing mode and the anti-symmetric polar wave is due to the collective coordinate description of the domain wall using only two parameters X and W, i.e., only the domain wall position and width are allowed to vary and other distortions are forbidden.

Propagation of Polar Waves along Ferroelectric Domain Wall. When the 1D ferroelectric domain wall is extended to 2D along y direction, the point-like domain wall object becomes a line-shaped domain wall along y direction. Accordingly, Eq. (3) is modified by replacement $\partial_x^2\to\partial_x^2+\partial_y^2$. With the extra y dimension, the bound state polar wave is also endowed with new freedom. In terms of the wave vector in the y direction (k_y), the symmetric and anti-symmetric bound state polar wave modes have dispersions expressed as follows:

$$\omega_{\rm s}(k_y)=ck_y,\quad \omega_{\rm a}(k_y)=\sqrt{\frac{3\omega_0^2}{4}+c^2k_y^2}, \tag{7}$$

where $c=\sqrt{\kappa/m}$ is the "speed of light" for the polar wave. Because the frequencies of these two modes are below the bulk gap ω_0, the ferroelectric domain wall is naturally a waveguide for these two propagating polar wave modes.

Furthermore, the domain wall position and width become y-dependent with $X(y,t)$ and $W(y,t)$, and their dynamics are governed by

$$m_X\frac{\partial^2 X}{\partial t^2}+\gamma_X\frac{\partial X}{\partial t}-\kappa_X\frac{\partial^2 X}{\partial y^2}=E(X)Q, \tag{8a}$$

$$m_W\frac{\partial^2 W}{\partial t^2}+\gamma_W\frac{\partial W}{\partial t}-\kappa_W\frac{\partial^2 W}{\partial y^2}=R(W)+E'(X)D, \tag{8b}$$

where $\kappa_X=4\kappa P^2/3W_0$ and $\kappa_W=(\pi^2-6)\kappa P^2/9W_0$ are the effective coupling constant of vibration mode and breathing mode, $Q=\int q_X(x)dx=-2P$ is the effective charge for vibration mode, $E(X)$ is the external electric field at the domain wall applied along the electric polarization direction, $D=\int xq_W(x)dx=-\pi^2W_0P/6$ is the effective dipole for breathing mode, and $E'(X)$ is the external electric field gradient acting on the dipole D. Equation (8) defines two wave equations for waves propagating along the domain wall extending y-direction. This is very much like waves on a string, with the domain wall being the string. Consequently, the domain wall extending in y-direction can be regarded as a waveguide with two distinct propagating polar wave modes, whose dispersions are given by Eq. (7).

To qualitatively investigate the propagation of polar wave along ferroelectric domain wall, we perform numerical simulation based on COMSOL Multiphysics, with the time evolution model solved using the generalized alpha method. In numerical simulations, we consider the bulk $BaTiO_3$ in tetragonal phase with following phase-field parameters:[17] the Landau phenomenological parameters $\alpha=2.77\times10^7\,\mathrm{V{\cdot}m/C}$, $\beta=1.7\times10^8\,\mathrm{V{\cdot}m^5/C^3}$, the coupling constant $\kappa=5.1\times10^{-10}\,\mathrm{J{\cdot}m^3/C^2}$, the damping constant $\gamma=2.5\times10^{-6}\,\mathrm{V{\cdot}m{\cdot}s/C}$, and the effective mass $m=1.3\times10^{-16}\,\mathrm{V{\cdot}m{\cdot}s^2/C}$. The bulk frequency gap for polar wave is then $\omega_0\approx0.653\,\mathrm{THz}$, and the anti-symmetric mode frequency gap is $\omega_{\rm a}\approx0.565\,\mathrm{THz}$.

In Fig. 2(a), the symmetric polar wave with frequency $\omega=0.2\,\mathrm{THz}$ ($\omega<\omega_{\rm a}<\omega_0$) is excited on the left edge of 1 nm width, and the polar wave is shown to propagate freely along the domain wall. Similarly, the anti-symmetric polar wave with frequency $\omega=0.65\,\mathrm{THz}$ ($\omega_{\rm a}<\omega<\omega_0$) is injected in Fig. 2(b), and the generated polar wave is also constricted within the domain wall. The constriction of the symmetric mode is better than the anti-symmetric mode, due to its much lower frequency gap, as shown in Eq. (4).

The profile of total electric polarization, including both the domain wall background and the bound state polar waves in Figs. 2(c) and 2(d), is demonstrated in Figs. 2(a) and 2(b). Apparently, the symmetric/anti-symmetric polar wave leads to a modulation of po-

sition/width of the domain wall, as expected from the correspondence between bound state and domain wall soft modes as discussed above. The domain wall position $X(y)$ and width $W(y)$ extracted from Figs. 2(c) and 2(d) are further plotted in Figs. 2(e) and 2(f), which agrees well with the numerical calculations based on Eq. (8).

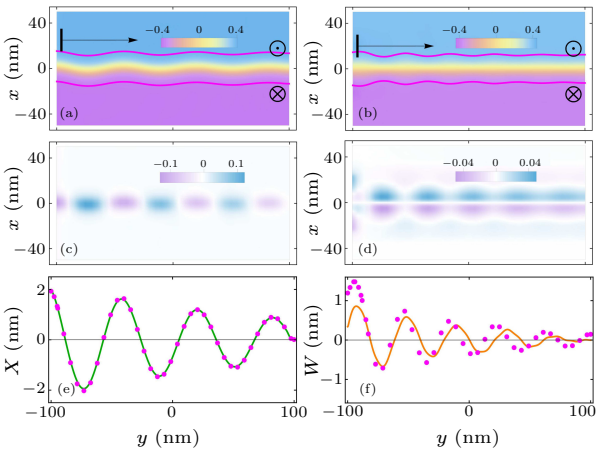

Fig. 2. Propagation of a polar wave along the ferroelectric domain wall. [(a), (b)] Snapshots of polar waves along domain wall with the static domain wall background included in a film in size 200 nm × 100 nm. In (a), an oscillating electric field with frequency $\omega = 0.2$ THz and amplitude $E_0 = 5 \times 10^6$ V/m is uniformly applied at the left edge of 1 nm width to generate symmetric polar wave; and in (b), an oscillating electric field with frequency $\omega = 0.65$ THz and spatial profile $E(x) = Kx$ with $K = 2 \times 10^{14}$ V/m^2 is applied to generate anti-symmetric polar wave. [(c), (d)] Snapshots of the polar waves with the electric polarization of the static domain wall subtracted corresponding to (a) and (b), respectively. [(e), (f)] The profile of domain wall position X and with W as functions of y. The solid lines are calculated from Eq. (8), and the dots are extracted from (a) and (b).

Influence of Impurities. Impurities are unavoidable in realistic materials, and are expected to affect the behavior of both the polar wave and ferroelectric domain wall.[34–36] We model the impurity as an additional pinning potential with $V_{\rm I} = \sum_i gp^2\delta(\boldsymbol{r} - \boldsymbol{r}_i)/2$, where $\boldsymbol{r}_i$ are the position of the impurities, and g is the pinning strength. Including the impurity effect, the LKT equation is then modified to

$$m\frac{{\rm d}^2p}{{\rm d}t^2} = -\gamma\frac{{\rm d}p}{{\rm d}t} + \kappa\nabla^2 p - \alpha p + \beta p^2 + E + gp\delta(\boldsymbol{r} - \boldsymbol{r}_i). \tag{9}$$

Due to the locality of the impurity effect, the domain wall and polar wave basically maintain their behaviors except at these pinning sites.

Consider a ferroelectric domain wall passing through a single impurity located at $\boldsymbol{r}_0 = (0, 0)$. The domain wall profile is unaltered, while the polar dynamics is additionally subject to a point potential $V_{\rm I} = gp\delta(\boldsymbol{r})$. The scattering problem of such point-potential is complicated, therefore we turn to the domain wall distortion model in Eq. (8), which is modified to

$$m_X\frac{\partial^2 X}{\partial t^2} + \gamma_X\frac{\partial X}{\partial t} - \kappa_X\frac{\partial^2 X}{\partial y^2} = EQ + F_{\rm PIN}(X)\delta(y), \tag{10}$$

with

$$F_{\rm PIN}(X) = -(gP^2/W_0)\,{\rm sech}^2(X/W_0)\tanh(X/W_0)$$

being the pinning force acting on domain wall. Around the equilibrium position $X = 0$, the pinning force is a linear restoring force $F_{\rm PIN}(X) \approx -gP^2X/W_0^2$. The antisymmetric breathing mode is not directly affected by the local impurity, thus is neglected in the following discussions.

Based on Eq. (10), we calculate the transmission probability when the vibration mode (symmetric bound state) scatters with this impurity as

$$T = \frac{1}{1 + (g/g_0)^2}, \tag{11}$$

where $g_0 = 8\kappa k_y W_0/3$ is the pinning strength corresponding to the transmission probability of $T = 0.5$. The transmission probability is controlled by the pinning strength g, as well as the wave vector k_y of the vibration mode.

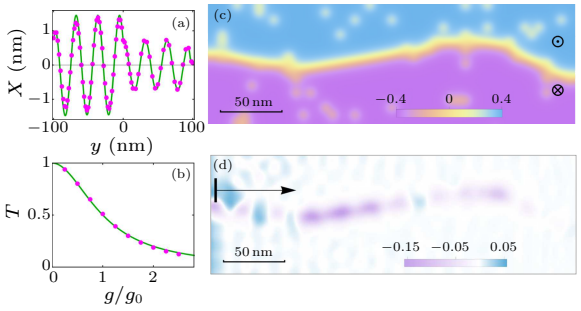

Fig. 3. Propagation of polar wave along the ferroelectric domain wall in the presence of impurities. (a) Profile of the symmetric polar wave scattered by a single pinning site. (b) The transmission probability as a function of pinning strength. The solid line is for theoretical value in Eq. (11), and the dots are extracted from numerical simulations. (c) The stabilized domain wall profile after relaxation. The impurities are randomly introduced inside the ferroelectric film, with averaged pinning strength of g_0. (d) The snapshot of polar wave propagated along the domain wall, with the electric polarization of the static domain wall subtracted.

The transmission probability of the vibration mode along the domain wall with a single pinning site is further investigated by numerical simulations. As demonstrated in Figs. 3(a) and 3(b), the transmission probability T extracted from the LKT equation based simulations agrees well with theoretical values in Eq. (11). For a remarkable range of pinning strength g, the reflection of bound state polar wave is weak, indicating the robustness of the guiding functionality.

We proceed to investigate the influence of multiple impurities on the polar wave propagation along the

domain wall. In Fig. 3(c), random impurities are included in the numerical simulations, and a straight domain wall is prepared at $x = 0$ for further relaxation. After relaxation, the domain wall is then captured locally by these impurities, and becomes winding, as shown in Fig. 3(c). An oscillating electric field with frequency $\omega = 0.5\,\text{THz}$ and amplitude $E_0 = 1 \times 10^7\,\text{V/m}$ is then exerted at the left side of the film, thus the generated polar wave (or vibration mode) is well below the bulk frequency gap. The polar wave excited by the electric field is again highly constricted by the ferroelectric domain wall as propagation, and only experiences very little leaking and reflection. The bound state polar wave is shown in Fig. 3(d), with the vibration of domain wall along the propagation clearly identified. The constricted propagation of polar wave along the winding domain wall indicates that the self-adjusted domain wall still functions well as a waveguide.

Discussions and Conclusions. In this work, we focus on a 180° up-down domain wall based on the minimal p^4 model of ferroelectricity, but all results naturally apply for more general types of domain wall or other ferroelectric models, such as 90°, 109° domain wall or p^6 model.[6,37–40] It is also known that the charged ferroelectric domain wall serves as channels for conduction electrons, due to the modification of local chemical potential.[41–45] In contrast, the polar wave investigated here does not involve the physical motion of electrons, thus can propagate even when the domain wall remains to be insulating.

In conclusion, we show that the ferroelectric domain wall acts as a waveguide for a polar wave, which is a collective excitation of electric polarization, similar to its magnetic counterpart. One symmetric and one antisymmetric bound state modes are identified within the ferroelectric domain wall, and they alternatively correspond to the vibration and breathing of domain wall itself. The waveguide functionality is robust again local impurities, and even survives when the shape of ferroelectric domain wall is modified substantially. The polar wave constricted within ferroelectric domain wall, offers new possibilities of transmitting electric signals in ferroelectric materials.

References

[1] Arnaud J 1980 *Opt. Quantum Electron.* **12** 187
[2] Refi J J 2002 *Bell Labs Tech. J.* **4** 246
[3] Voiculescu I and Nordin A N 2012 *Biosens. Bioelectron.* **33** 1
[4] Khitun A, Bao M and Wang K L 2010 *J. Phys. D* **43** 264005
[5] Wagner K, Kákay A, Schultheiss K, Henschke A, Sebastian T and Schultheiss H 2016 *Nat. Nano.* **11** 432
[6] Catalan G, Seidel J, Ramesh R and Scott J F 2012 *Rev. Mod. Phys.* **84** 119
[7] Krawczyk M and Puszkarski H 2006 *Cryst. Res. Technol.* **41** 547
[8] Marrows C 2005 *Adv. Phys.* **54** 585
[9] Garcia-Sanchez F, Borys P, Soucaille R, Adam J P, Stamps R L and Kim J V 2015 *Phys. Rev. Lett.* **114** 247206
[10] Lan J, Yu W, Wu R and Xiao J 2015 *Phys. Rev. X* **5** 041049
[11] Beach G S, Nistor C, Knutson C, Tsoi M and Erskine J L 2005 *Nat. Mater.* **4** 741
[12] Boulle O, Malinowski G and Kläui M 2011 *Mater. Sci. Eng. R* **72** 159
[13] Kläui M, Vaz C, Bland J, Wernsdorfer W, Faini G, Cambril E and Heyderman L 2003 *Appl. Phys. Lett.* **83** 105
[14] Parkin S S, Hayashi M and Thomas L 2008 *Science* **320** 190
[15] Meyer B and Vanderbilt D 2002 *Phys. Rev. B* **65** 104111
[16] Seidel J 2012 *J. Phys. Chem. Lett.* **3** 2905
[17] Chotorlishvili L, Khomeriki R, Sukhov A, Ruffo S and Berakdar J 2013 *Phys. Rev. Lett.* **111** 117202
[18] Wu X, Petralanda U, Zheng L, Ren Y, Hu R, Cheong S W, Artyukhin S and Lai K 2017 *Sci. Adv.* **3** e1602371
[19] Yang T, Wang B, Hu J M and Chen L Q 2020 *Phys. Rev. Lett.* **124** 107601
[20] Li Q, Stoica V A, Paściak M, Zhu Y, Yuan Y, Yang T, McCarter M R, Das S, Yadav A K, Park S, Dai C, Lee H J, Ahn Y, Marks S D, Yu S, Kadlec C, Sato T, Hoffmann M C, Chollet M, Kozina M E, Nelson S, Zhu D, Walko D A, Lindenberg A M, Evans P G, Chen L Q, Ramesh R, Martin L W, Gopalan V, Freeland J W, Hlinka J and Wen H 2021 *Nature* **592** 376
[21] Tani K 1969 *J. Phys. Soc. Jpn.* **26** 93
[22] Ishibashi Y 1989 *Ferroelectrics* **98** 193
[23] Ishibashi Y 1990 *Ferroelectrics* **104** 299
[24] Sivasubramanian S, Widom A and Srivastava Y 2004 *Ferroelectrics* **300** 43
[25] Widom A, Sivasubramanian S, Vittoria C, Yoon S and Srivastava Y N 2010 *Phys. Rev. B* **81** 212402
[26] Giri P, Choudhary K, Gupta A S, Bandyopadhyay A and McGurn A R 2011 *Phys. Rev. B* **84** 155429
[27] Khomeriki R, Chotorlishvili L, Malomed B and Berakdar J 2015 *Phys. Rev. B* **91** 041408
[28] Cao W and Cross L E 1991 *Phys. Rev. B* **44** 5
[29] Bandyopadhyay A, Ray P and Gopalan V 2006 *J. Phys.: Condens. Matter* **18** 4093
[30] Hlinka J and Márton P 2006 *Phys. Rev. B* **74** 104104
[31] Merz W J 1954 *Phys. Rev.* **95** 690
[32] Lee D, Behera R K, Wu P *et al.* 2009 *Phys. Rev. B* **80** 060102
[33] Pöschl G and Teller E 1933 *Z. Phys.* **83** 143
[34] Rodriguez B J, Chu Y, Ramesh R and Kalinin S V 2008 *Appl. Phys. Lett.* **93** 142901
[35] Yang T, Gopalan V, Swart P and Mohideen U 1999 *Phys. Rev. Lett.* **82** 4106
[36] Rojac T, Kosec M, Budic B, Setter N and Damjanovic D 2010 *J. Appl. Phys.* **108** 074107
[37] Ishibashi Y and Salje E 2002 *J. Phys. Soc. Jpn.* **71** 2800
[38] Rao W F and Wang Y U 2007 *Appl. Phys. Lett.* **90** 041915
[39] Lubk A, Gemming S and Spaldin N 2009 *Phys. Rev. B* **80** 104110
[40] Schilling A, Byrne D, Catalan G, Webber K, Genenko Y, Wu G, Scott J and Gregg J 2009 *Nano Lett.* **9** 3359
[41] Seidel J, Martin L W, He Q *et al.* 2009 *Nat. Mater.* **8** 229
[42] Eliseev E A, Morozovska A N, Svechnikov G S, Gopalan V and Shur V Y 2011 *Phys. Rev. B* **83** 235313
[43] Farokhipoor S and Noheda B 2011 *Phys. Rev. Lett.* **107** 127601
[44] Maksymovych P, Seidel J, Chu Y H, Wu P, Baddorf A P, Chen L Q, Kalinin S V and Ramesh R 2011 *Nano Lett.* **11** 1906
[45] Schröder M, Haußmann A, Thiessen A, Soergel E, Woike T and Eng L M 2012 *Adv. Funct. Mater.* **22** 3936